Optical Engineering

OpticalEngineering.SPIEDigitalLibrary.org

Point-based and model-based geolocation analysis of airborne laser scanning data

Umut Gunes Sefercik
Gurcan Buyuksalih
Karsten Jacobsen
Mehmet Alkan

SPIE.

Umut Gunes Sefercik, Gurcan Buyuksalih, Karsten Jacobsen, Mehmet Alkan, "Point-based and model-based geolocation analysis of airborne laser scanning data," *Opt. Eng.* **56**(1), 013101 (2016), doi: 10.1117/1.OE.56.1.013101.

Point-based and model-based geolocation analysis of airborne laser scanning data

Umut Gunes Sefercik,[a] Gurcan Buyuksalih,[b] Karsten Jacobsen,[c] and Mehmet Alkan[d,*]
[a]Bulent Ecevit University, Department of Geomatics Engineering, Zonguldak 67100, Turkey
[b]IMP Bimtas, Tophanelioglu Street, Istanbul 34430, Turkey
[c]Leibniz University Hannover, Institute of Photogrammetry and Geoinformation, Nienburger Street 1, Hannover D-30167, Germany
[d]Yildiz Technical University, Department of Geomatics Engineering, Istanbul 34220, Turkey

Abstract. Airborne laser scanning (ALS) is one of the most effective remote sensing technologies providing precise three-dimensional (3-D) dense point clouds. A large-size ALS digital surface model (DSM) covering the whole Istanbul province was analyzed by point-based and model-based comprehensive statistical approaches. Point-based analysis was performed using checkpoints on flat areas. Model-based approaches were implemented in two steps as strip to strip comparing overlapping ALS DSMs individually in three subareas and comparing the merged ALS DSMs with terrestrial laser scanning (TLS) DSMs in four other subareas. In the model-based approach, the standard deviation of height and normalized median absolute deviation were used as the accuracy indicators combined with the dependency of terrain inclination. The results demonstrate that terrain roughness has a strong impact on the vertical accuracy of ALS DSMs. From the relative horizontal shifts determined and partially improved by merging the overlapping strips and comparison of the ALS, and the TLS, data were found not to be negligible. The analysis of ALS DSM in relation to TLS DSM allowed us to determine the characteristics of the DSM in detail. [DOI: 10.1117/1.OE.56.1.013101]

Keywords: airborne laser scanning; terrestrial laser scanning; height; digital surface model; accuracy.

Paper 160944 received Jun. 16, 2016; accepted for publication Oct. 31, 2016; published online Dec. 1, 2016.

1 Introduction

In the last few decades, advanced airborne and space-borne remote sensing technologies have become indispensable, particularly for land-related professions requiring rapid, periodical, and high-accuracy three-dimensional (3-D) geoinformation. Airborne systems offer higher resolution than space-borne methods since they can perform measurements at lower altitudes. Airborne laser scanning (ALS), in particular, can identify high-resolution point clouds using 3-D ground coordinates. From the derived points, a digital surface model (DSM), which is the 3-D presentation of the entire vegetation and man-made objects in the observation area, and a digital terrain model (DTM), which is related to the bare ground and interpolates the earth surface and locations of buildings, are generated. DSM and DTM can be identified also with the general inclusive term digital elevation model (DEM). With the advantage of providing 3-D and precise data, ALS has been adopted as one of the primary techniques for mapping local to national scale coverage, a topic historically dominated by photogrammetry[1,2] and utilized in several DEM-based studies.[3–12]

Considering the large utilization of ALS DEMs, their geolocation accuracy remains a significant question. This study was designed to answer to this question by producing very high resolution (VHR) ALS DSMs in several study areas, which have varied terrain formations, and validating them through visual and statistical approaches and geometric tests regarding the function of terrain slope. In ALS, the accurate detection of geolocation depends on several parameters such as flying altitude above ground, footprint size, and terrain roughness. In the literature, the quality of the ALS DSM is mostly assessed by a checkpoint-based comparison.[13–18] However, checkpoints have special location attributes, which usually do not represent the whole height model. For a complete and most reliable geolocation accuracy evaluation including all of the pixels of ALS raster DSMs, the checkpoint-based analysis was combined with model-to-model approaches that allow a 3-D-comparison of the ALS DSMs strip to strip internally and the terrestrial laser scanning (TLS) DSMs.

This paper is organized as follows: Section 2 presents information about the study areas in Istanbul and the materials used; it is followed by the methodology section, which summarizes the ALS DSM generation and accuracy validation steps. The experimental results are presented and discussed according to the mapping requirements in Sec. 4. Finally, Sec. 5 presents the conclusion of the study.

2 Study Areas and Materials

The greater municipality of Istanbul implemented a project from 2012 to 2013 to collect ALS data over a 5400-km^2 area to generate a 3-D model of the city based on a DSM and DTM. For a model-based quality analysis, seven study areas with varying terrain characteristics were selected mainly from the European side of Istanbul (Fig. 1). In test areas 1 to 3, the overlap areas of the neighboring flight lines were compared and in areas 4 to 7, the TLS data were used as references. ALS was performed using a helicopter equipped with a Riegl laser scanner Q680i, and the TLS

*Address all correspondence to: Mehmet Alkan, E-mail: alkan@yildiz.edu.tr

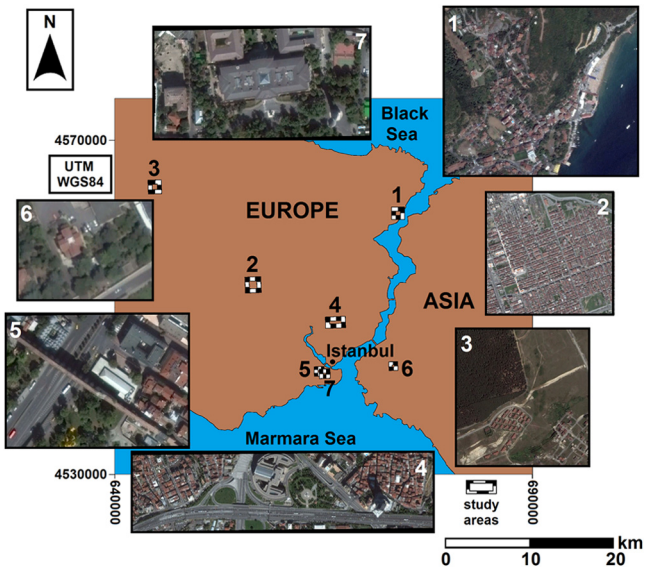

Fig. 1 Location of the test areas in Istanbul.

data were obtained from Riegl VZ-400. The detailed information about ALS and TLS measurements and instruments are given in Table 1.

3 Methodology

For the validation of the ALS accuracy, five main steps were used (Fig. 2). The common commercial software package, TerraSolid for MicroStation (v14), was chosen to process the ALS data in .las format.[19,20] For the generation of DSMs, 3-D transformation, and accuracy analysis, Surfer (v11) and the program system Bundle Block Adjustment Leibniz University of Hannover (BLUH) were utilized. In the course of the analysis, the coordinate system was UTM zone 35 based on WGS84 datum.

3.1 *Improvement of Airborne Laser Scanning Point Clouds*

The acquisition of ALS point clouds is based on direct sensor orientation and boresight alignment. For the relative kinematic global navigation satellite system (GNSS) positioning of direct sensor orientation, at least eight satellites with a position dilution of precision value below 2.5 were used for every flight line, and the processing indicated that the standard deviation (σz) in the Z-direction was between 4 and 7 cm. In addition, the boresight alignment, laser scanner, and definition of an object "point" had an impact on the data. Crossing flight lines can be used for the block handling of ALS strips supported by ground control points (GCPs), but in this project, such crossing flight lines were not available and for the high number of linear flight lines, collecting a GCP for every line is not realistic. Therefore, subblocks of ~10 flight lines were built. With TerraMatch included in the TerraSolid application, ~50% of the lateral overlapping strips of the different flight lines were three-dimensionally transformed together and the areas were monitored based on the extracted inclined planes with at least a 10-deg

Table 1 Specifications of the ALS and TLS measurements and instruments.

Parameter	Airborne laser scanning	TLS areas 4 to 7
Instrument	Riegl LS Q680i	Riegl VZ-400
Dates of flight/ground survey	Area 4: October 12, 2012	Area 4: July 16 to 17, 2012
	Area 5: September 30, 2012	Area 5: August 17, 2013
	Area 6: September 23, 2012	Area 6: July 10, 2013
	Area 7: October 3, 2012	Area 7: June 30 + July 10, 2013
Flying altitude	600 m	—
Laser footprint	30 cm at 600 m	3 cm at 100 m
Average point density (per 1 m^2)	20	~10,000 points ≤ 10 m
Field of view (deg)	−30 deg to +30 deg	360 deg horizontal/ − 40 deg to +60 deg vertical
Pulse rate	400 kHz	300 kHz
Wavelength	1550 nm	1550 nm
Scan frequency	200 Hz	N/A
Beam divergence	0.5 mrad	0.35 mrad
Number of returns	4	4
Velocity of helicopter	150 km/h	—
Integrated mid-format digital camera	IGI DigiCam 60 (50-mm focal length)	—

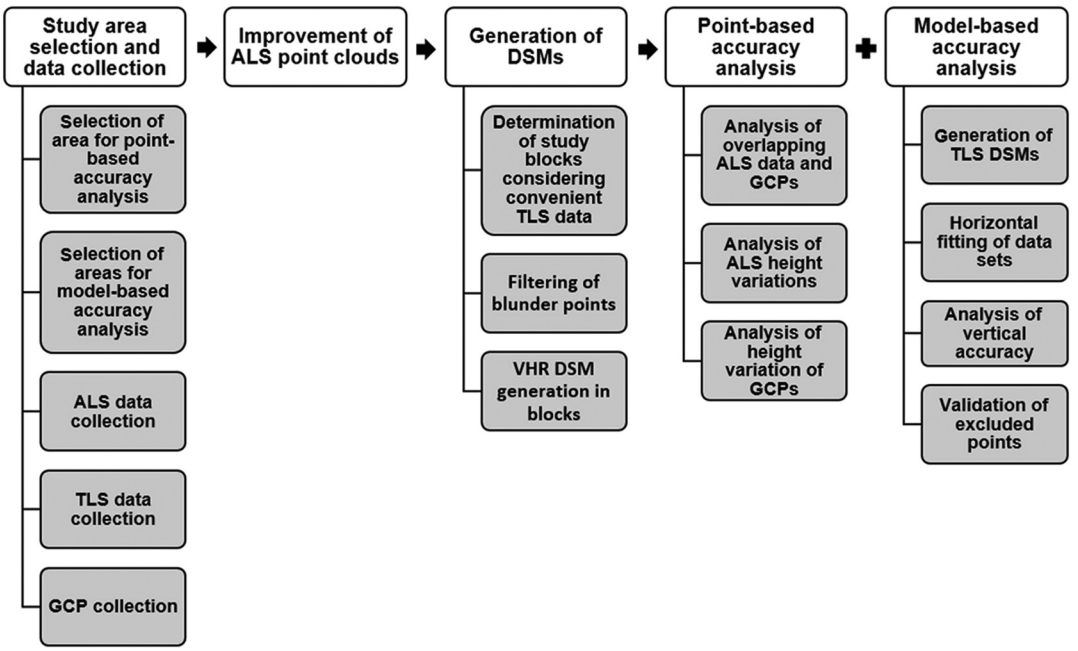

Fig. 2 Methodology.

Variations	RMSE	Test area
ALS DSM – checkpoints	3.3 cm (bias=0.3 cm)	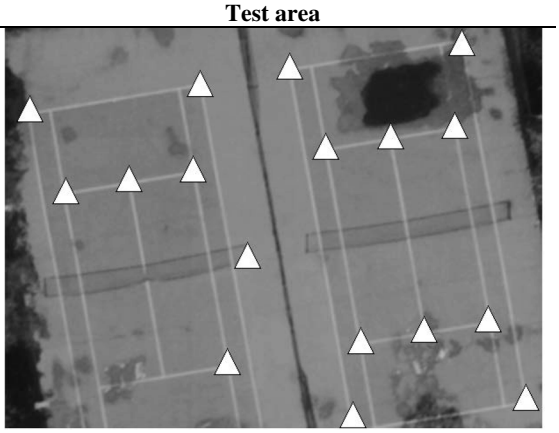
height variation of the checkpoints determined by GNSS	+/- 3 cm	
height variation of the ALS data	+/- 1.4 cm	

Fig. 3 Checkpoint distribution on the tennis court.

inclination. Such inclined planes, usually roofs of buildings, allow not only vertical but also horizontal fitting.[21] Such planes are not much affected by roughness.

3.2 *Point-Based Geolocation Accuracy Analysis*

Point-based accuracy analysis is the simplest way to determine the vertical system accuracy of ALS point clouds.[22] However, considering the nearly continuous nature of an ALS point cloud, it is not possible to estimate the absolute accuracy of point clouds in a rough terrain using a limited number of checkpoints. On this basis, point-based geometric test of the merged ALS point clouds was utilized to estimate ALS geolocation accuracy in flat areas. The process was conducted with 17 checkpoints on a tennis court (Fig. 3).

The expected accuracy depends upon the σz of the laser range of nominal {plus minus} 2 cm, the accuracy of the scan angle {plus minus} 0.003 deg, the inertial measurement unit (IMU) roll and pitch {plus minus} 0.003 deg, the IMU heading {plus minus} 0.01 deg, and the relative kinematic positioning {plus minus} 5 cm. For the {plus minus} 30-deg field of view, the influence of the relative kinematic positioning on the height of the determined object was in the same range as all the effects of the attitudes at the ALS strip limit for the 600-m flying elevation, leading to an approximate σz of 7.5 cm in the Z-direction. This was improved by fitting and merging the overlap areas of the neighboring subblocks of strips by GCPs.

3.3 *Model-Based Geolocation Accuracy Analysis*

Model-based analysis is based on the differences between the ALS DSMs and the reference DSMs, rather than the use of a limited number of checkpoints. This is a more realistic

technique for the accuracy analysis of a DSM.[23] The reference model has to be achieved using the same or a more precise technique as that of the tested model, and its original grid spacing has to be at least equal or smaller. Considering these criteria, ALS and TLS data are the most appropriate references for the analysis of the ALS data.[24] In this study, DSMs, derived from ~50% overlapping ALS strips, were compared internally. In addition, DSMs, achieved from matched and merged ALS strips, were checked against the TLS DSMs.

In addition to σz, the normalized median absolute deviation (NMAD) [Eq. (2)] was used as an accuracy criterion. NMAD is the derivative of median absolute deviation (MAD) [Eqs. (1) and (2)]. σz and NMAD are the main accuracy criteria facilitating the validation and specification of outliers. Both accuracy figures are identical if the evaluated discrepancies are normally distributed; however, this is usually not the case.[25] In Eq. (1), $\tilde{x}_i$ is the median of absolute height discrepancies between the two DEMs.

σz is related to average while root-mean-square errors (RMSE) are influenced by the bias. Due to the square sum nature of σz, it is strongly affected by larger discrepancies. NMAD is based on the median, so it does not change much if the error frequency distribution does not correspond to a normal distribution. However, the normal distribution of the discrepancies is usually limited, in which case NMAD describes the frequency distribution of discrepancies better, usually being smaller than σz. The correct description of the vertical accuracy of a height model is based on the Euclidian distances, the shortest distance between height models, depending upon the cosine of the terrain inclination. In our investigation, the Euclidian standard deviation was nearly the same as σz in the vertical direction. More than those used in this study, several estimators such as relative bias, average relative absolute difference (ARAD), and log RMSE are generally utilized for the accuracy validation of DEMs derived from remotely sensed data.[26]

$$\mathrm{MAD} = \tilde{x}_i[|\Delta Z_i|], \tag{1}$$

$$\mathrm{NMAD} = 1.4815 \times \mathrm{MAD}. \tag{2}$$

At the first step of the model-based analysis, in three study areas, 9 DSMs were generated in nine strips and validated by being comparing with each other in ~50% overlapping parts of the strips. In the second step, completing the TLS measurements in four areas, the reference data were obtained for the merged ALS data. Figure 4 shows the ALS classification (color-coded) and TLS point-clouds (black and white) in the four test areas with orthometric height scales. In area 4, the TLS data were obtained from mobile mapping. The ALS and TLS DSMs were generated by TerraScan in TerraSolid. Required interpolations were based on kriging.[27] The horizontal offsets between the ALS and TLS DSMs were eliminated by shifting based on an area-matching cross correlation.

In addition to the absolute standard deviation ($A\sigma z$), relative standard deviation ($R\sigma z$) indicating the interior consistency of a DSM based on the relationship between the neighboring grids was calculated separately for each area. The distance of the current point to a reference point indicates height differences, which are compared for all

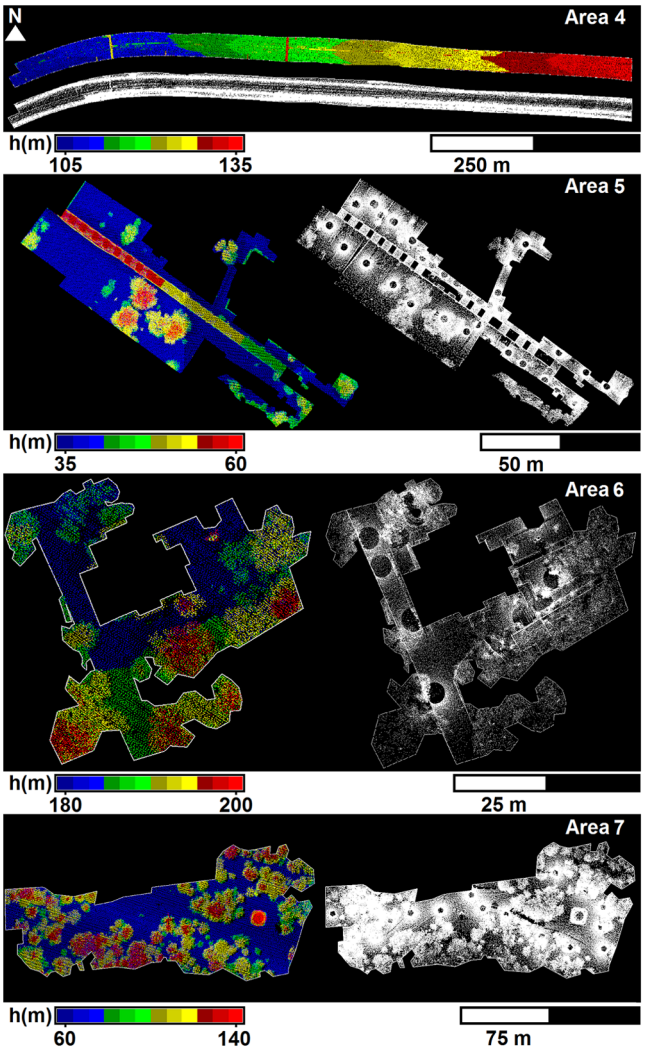

Fig. 4 Point clouds in the test areas 4 to 7; ALS terrain classification using absolute elevation (in color), TLS point clouds (black and white).

neighboring grids. In the case of independent height differences (correlation = 0), $R\sigma z$ would be identical to σz, and if the correlation coefficient is 1.0, $R\sigma z$ would be zero. Therefore, under normal conditions, $R\sigma z$ is between zero and σz. However, in the extreme case of a negative correlation, the $R\sigma z$ may be larger than σz. Using $R\sigma z$, the dependency (correlation) of the height differences between the tested and reference models (DZ) is checked, through which local systematic errors and random errors can be differentiated. It has been reported that $R\sigma z$ of active remote sensing systems such as radar and lidar are superior to their $A\sigma z$.[28–30]

$R\sigma z$ of the DSMs were calculated using Eq. (3), where D represents the distance groups and D_l and D_u are the lower and upper distance limits. In this study, for each pixel, the neighboring 10 pixels were used in the calculation; therefore, the distance groups varied from the first to the tenth pixel (1 to 10 m based on a 1-m pixel size of the reference data and 0.5 to 5 m for 0.5 m reference data). nx indicates the number of point combinations in the distance group and n represents the total number of differences between the reference and actual values. A factor of 2 for multiplication with nx is used for norming $R\sigma z$ to the size of σz. If the

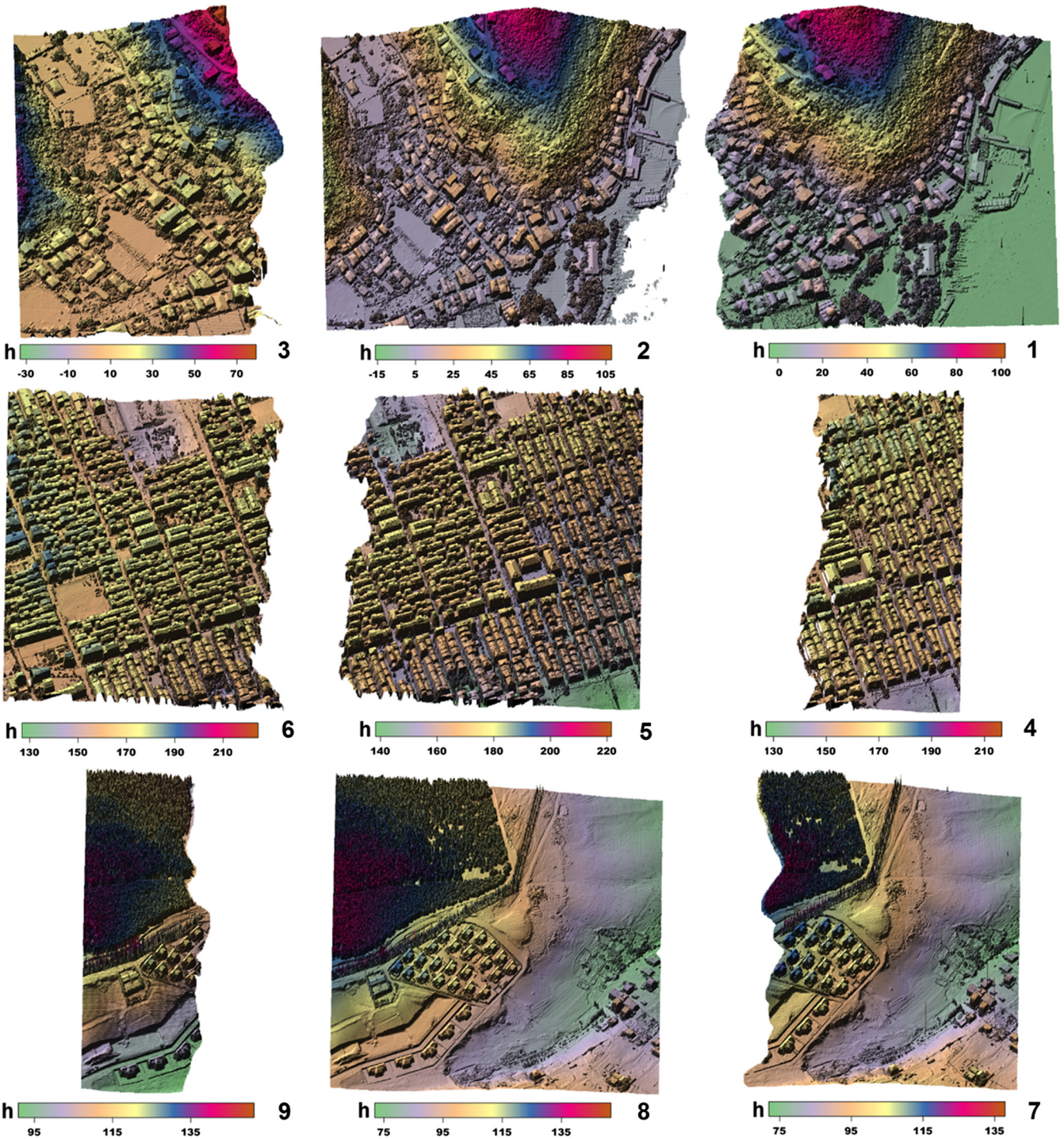

Fig. 5 0.5-m gridded DSMs of overlapping ALS strips for the test areas 1 to 3 (strips 1, 2, 3 = area 1; strips 4, 5, 6 = area 2; strips 7, 8, 9 = area 3).

height differences of the points in the distance group are independent, corresponding to the error propagation, then the RMS would be the square root of 2.0 larger than σz, which is represented by $2 \times nx$

$$R\sigma z = \sqrt{\frac{\sum (DZ_i - DZ_j)^2}{(2 \times nx)}} \quad \text{and} \quad D_l < D < D_u. \tag{3}$$

As expected, height models and the laser scan data are not as accurate in an inclined terrain as in flat areas. As known, when generating any kind of DEM, the interpolation is a crucial step for vector-raster transformation to assign a gray value for each pixel of the raster model. On the other hand, the interpolation causes geolocation accuracy loss on the raster model due to produce derivative gray values, which are not as reliable as the original point-clouds. The influence of interpolation in final 3-D product depends

Table 2 Accuracies of ALS DSMs derived from the combinations of ALS strips.

Strip combinations	σz (cm)	NMAD (cm)	Influence of roll to Z from one side to another (cm)
1 to 2	6.0	5.0	2.5
2 to 3	10.0	9.0	2.8
4 to 5	5.0	4.0	0.0
5 to 6	6.0	4.0	2.9
7 to 8	12.0	10.0	21.0
8 to 9	8.0	6.0	5.0
7 to 8 after rotation correction	8.0	7.0	1.5

on several parameters such as original grid spacing of the data, interpolation window size, used interpolation method, the characteristics of land cover (open, forest, etc.) and the inclination of the terrain.[31] In this study, the effect of slope on the accuracy was taken into account by $\sigma z = a + b \times \tan$ (terrain inclination) with a and b indicating the certain accuracy value and the factor of terrain inclination, respectively. The analysis describes the accuracy corresponding to this dependency. In this analysis, only height discrepancies within a realistic threshold are taken into account, the remaining data was handled as blunders. Here, a threshold of {plus minus} 1 m between ALS DSMs and reference DSMs was used and the percentage of blunders in all analyzed data was included in accuracy tables as excluded points. Blunders may be caused by growing vegetation related to the temporal spacing between the ALS and TLS data collection dates, and the different viewing geometry of the ALS and TLS scans showing different object parts in vegetation.

4 Results

4.1 *Results of Point-Based Analysis*

Figure 3 shows the RMS differences of ALS points against 17 checkpoints on the tennis court and the height variations of the checkpoints.

The small bias is a random result. However, the RMS differences in height (RMSE: 3.3 cm) and the internal height variation of ALS heights on the flat tennis court being only 1.4 cm indicate high relative accuracy. The height variation of the GNSS heights being 3 cm indicates lower accuracy of the reference measurement compared to the ALS heights.

4.2 *Results of Model-Based Analysis*

Figure 5 shows the overlapping ALS DSMs of the test areas 1, 2, and 3 with 50 cm grid spacing (color-coded). The direct comparison of the overlapping ALS heights is dominated by the random influence of vegetation and building outlines. At building outlines, points with the same X- and Y-location may be located on the roof overhang in one strip and on the facade in the other. Table 2 shows the results of ~50% overlapped ALS strips after shift correction with RiPROCESS in TerraSolid. Strips 1 to 3 are not the same as the test areas used for the comparison with the TLS data. The comparison of strip 7 with strip 8 indicates a clear rotation of these strips against each other. After the correction of this rotation, σz and NMAD were within the usual range. The values in Table 2 are clearly greater than the results obtained from the tennis court due to object roughness. Object roughness is not a problem for strip transformation by TerraSolid since it is based on inclined flat planes, e.g., building roofs.

Figure 6 shows the ALS and TLS DSMs in areas 4 to 7 after shift correction based on area-matching cross-correlation. The horizontal shifting values were found to range from −3.08 to 1.07 cm in the X-direction and from −6.00 to 0.18 cm in the Y-direction. The grid spacing of the DSMs was 1 m with the exception of area 6 where it was 0.5 m.

Figure 7 shows, in white, the points (pixels) that were excluded due to exceeding the 1-m threshold between the ALS and TLS. Particularly in vegetation, due to unstable geometry, different footprint locations and view directions lead irregular height values in point definition. Similar problems also exist on facades and roof overhang points. Moving cars are another reason for the excluding threshold. Apart from the exclusion method by determining a threshold, problematic points can be removed by using an appropriate filtering algorithm.

The frequency distributions of height differences between the ALS DSMs and TLS DSMs in Fig. 8 show the nonnegligible bias, requiring an optimal fit of the TLS to ALS data. In addition, the limited normal distribution is demonstrated. The large differences between σz and NMAD are caused by the higher number of larger discrepancies, influencing the square nature of σz more than the normalized median. Figure 9 shows the $R\sigma z$ of height differences in areas 4, 5, 6, and 7. The results vary from 12 to 25 cm, which indicates normal conditions for all the study areas. The correlation of neighboring pixels is very local with $R\sigma z$ not changing in distances exceeding 5 or less pixels. The results are superior to $A\sigma z$ as expected for active remote sensing systems.

With respect to the guidelines published by the American Society for Photogrammetry and Remote Sensing (ASPRS), the horizontal and vertical accuracy of the ALS DEMs were evaluated based on the produced map scale and contour interval according to the mapping requirements determined by United States National Map Accuracy Standards (NMAS) and National Standards for Spatial Data Accuracy (NSSDA) (Table 4). Horizontal shifting and model-based absolute vertical accuracy after the elimination of systematic bias demonstrate that the ALS DSMs fulfill the horizontal and vertical accuracy criteria of 1/1000 scaled topographic maps at the 95% confidence level (compare Tables 3 and 4).

5 Conclusion

In this study, the geo-location characteristics and accuracy of the ALS DSMs were analyzed using point-based and model-based approaches. The point-based analysis was conducted on a completely flat tennis court using checkpoints. This allowed the verification of the absolute and relative height level of the ALS height model but not the confirmation of the horizontal location. Absolute and $R\sigma z$ of the height were not representative for an undulating or rough terrain. Through

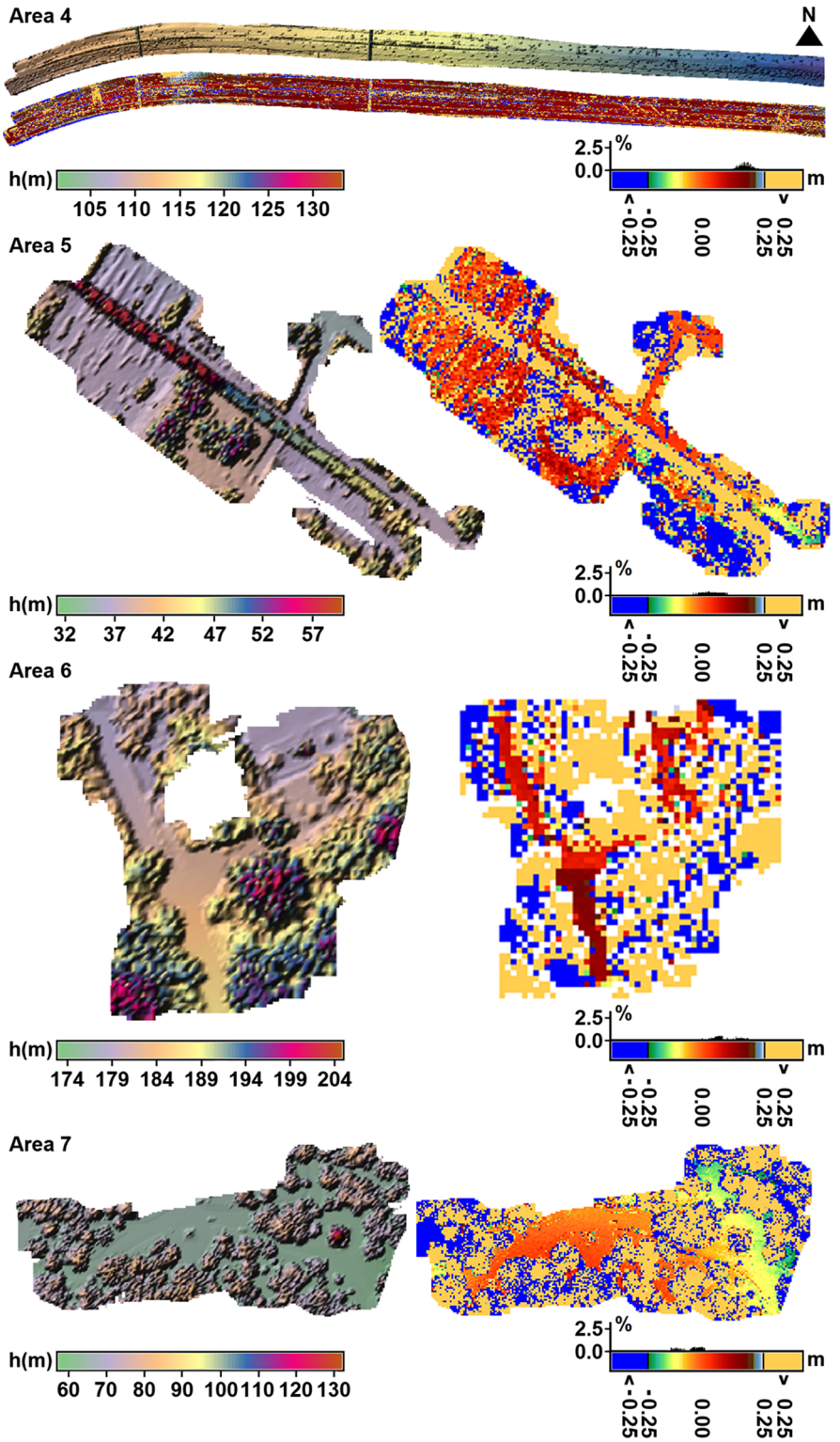

Fig. 6 Color-coded DSMs (left) and differential DEMs with bias (right); height and height difference scale (m).

the model-based analysis of the overlapping ALS strips, more realistic accuracy values were obtained, but the different viewing directions required the exclusion of vegetation areas as well as building outlines. The model-based analysis based on the comparison of ALS DSMs of the merged strips with the TLS DSMs presented similar problems in terms of the vegetation and building outlines, which required filtering.

The difference between σz of height and NMAD demonstrated a limited normal distribution of the height discrepancies, influencing σz more than NMAD. In addition, NMAD was found to demonstrate the frequency distribution of the height differences better than σz, due to the latter strongly depending upon larger discrepancies. It was clear that the accuracy depended upon terrain inclination, which required

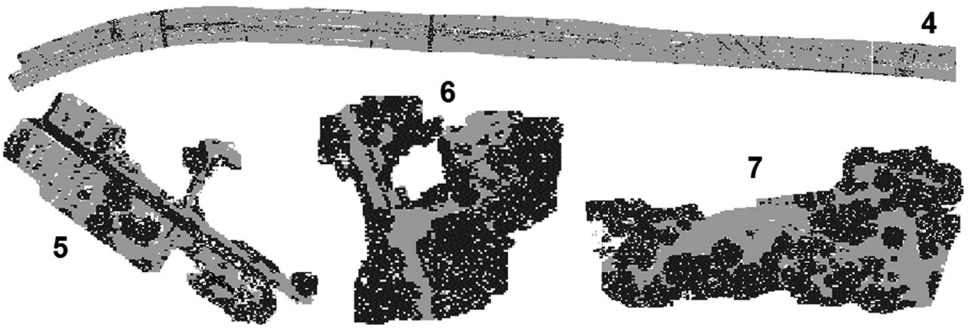

Fig. 7 Excluded points (in white) where $\Delta Z > 1$ m.

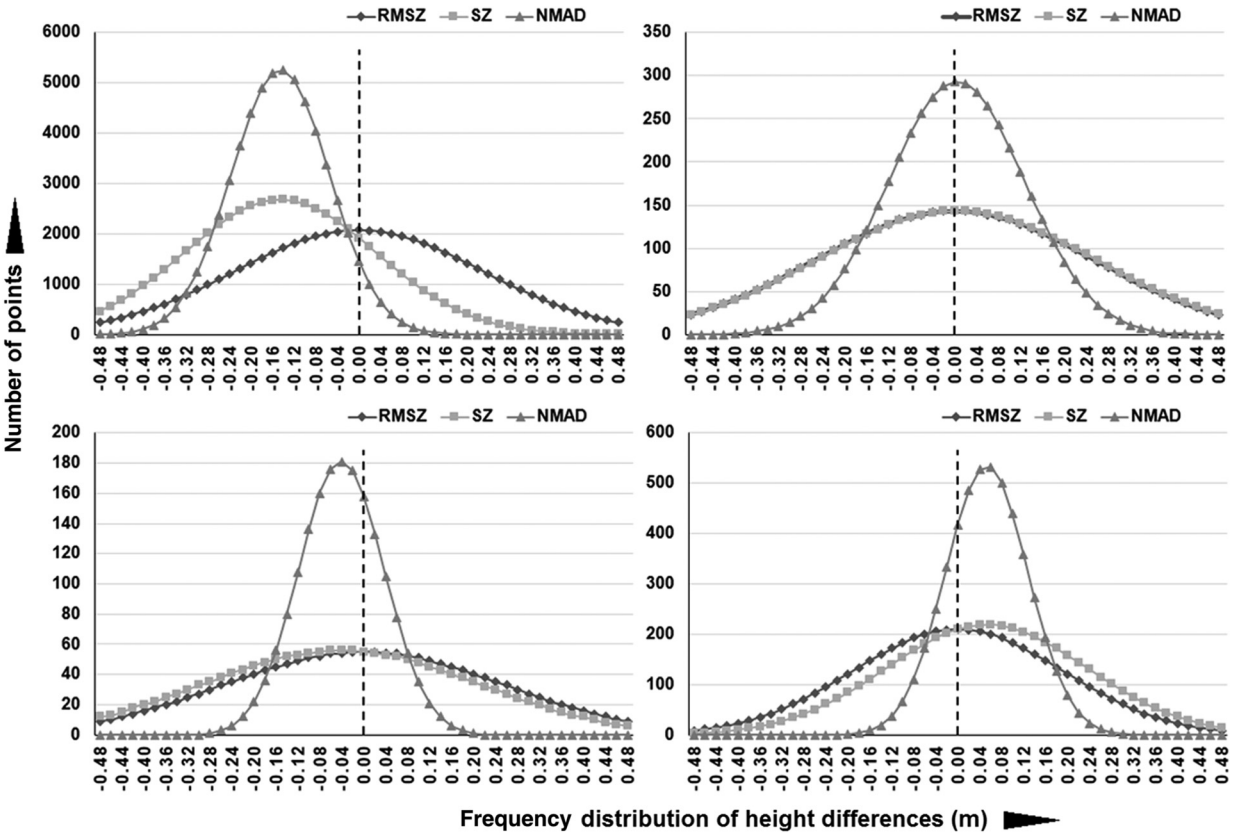

Fig. 8 Frequency distribution of height differences between the ALS and TLS DSMs before and after the optimal fitting of strips.

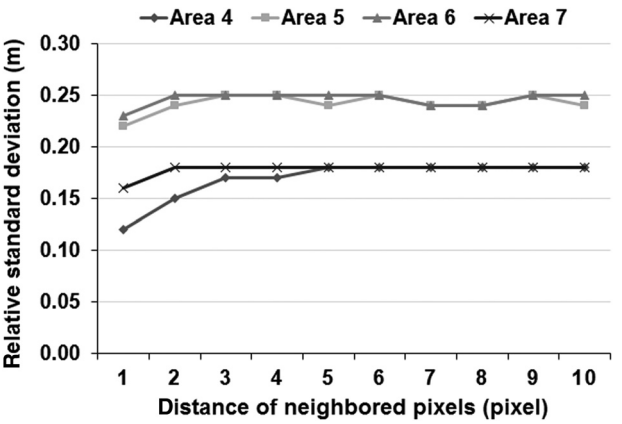

Fig. 9 $R\sigma z$ of the ALS DSMs.

the description of accuracy as a function of terrain inclination. In general, the vertical accuracy of the ALS DSM was around 3 cm in flat areas such as the tennis court, and NMAD ranged from 7 to 14 cm for a vegetated and rough terrain.

The model-based analysis also facilitated the determination of the horizontal position of the height model, which cannot be determined in flat areas. Overall, the large ALS DSM based on helicopter flights without crossing flight lines lead to satisfying results, confirming the strategy used. In areas of vegetation, the discrepancies between different datasets are dominated by the point definition caused by the footprint location not being the same and different view directions leading to varying height values also being points on facades and roof overhangs. In a rough terrain, such as cultivated land with low vegetation and uncultivated areas, the RMS differences between the height determination from

Table 3 Absolute vertical accuracy of ALS DSMs in relation to TLS DSMs (α = slope).

Area	Spacing (m)	Number of points	Bias (m)	RMSE (m)	σz (m)	NMAD (m)	σz as a function of slope (m)	Excluded points (%)
4	1	59,839	0.15	0.23	0.18	0.07	$0.22 + 0.10 \times \tan(\alpha)$	2.84
			0.00	0.19	0.19	0.07	$0.21 + 0.07 \times \tan(\alpha)$	2.36
5	1	4569	0.00	0.25	0.25	0.10	$0.23 + 0.09 \times \tan(\alpha)$	15.77
6	0.5	1774	0.04	0.25	0.25	0.03	$0.10 + 0.30 \times \tan(\alpha)$	21.33
			0.00	0.25	0.25	0.03	$0.08 + 0.35 \times \tan(\alpha)$	21.24
7	1	5336	0.05	0.19	0.18	0.08	$0.14 + 0.34 \times \tan(\alpha)$	20.63
			0.00	0.19	0.19	0.08	$0.15 + 0.26 \times \tan(\alpha)$	20.52

Table 4 Map accuracy requirements based on the map scale and contour interval.[29]

		Horizontal		Vertical	
Map scale	Contour interval (m)	RMS (cm)	Accuracy (95% confidence level) (1.96 × RMS) (cm)	RMS (cm)	Accuracy (95% confidence level) (1.96 × RMS) (cm)
1:500	0.5	0.28	0.55	4.60	9.10
1:1000	1	0.56	1.10	9.25	18.2
1:2000	2	1.12	2.20	18.5	36.3
1:5000	5	2.79	5.47	46.3	90.8

different flight lines and between ALS and TLS data more clearly show the definition of the object surface as the accuracy of laser scanning. The comparison of the ALS and TLS results is an excellent way of obtaining realistic information about object definition, especially in vegetated and rough areas as well as at building outlines. In terms of the ASPRS guidelines, the ALS DSMs fulfill the horizontal and vertical accuracy requirements of 1/1000 scaled topographic maps at the 95% confidence level.

References

1. E. Baltsavias, "A comparison between photogrammetry and laser scanning," *ISPRS J. Photogramm.* **54**(2), 83–94 (1999).
2. J. Hill et al., "Wide-area topographic mapping and applications using airborne light detection and ranging (Lidar) technology," *Photogramm. Eng. Remote Sens.* **66**(8), 908–914 (2000).
3. U. Lohr, "Digital elevation models by laser scanning," *Photogramm. Rec.* **16**(91), 105–109 (1998).
4. J. Shan and A. Sampath, "Urban DEM generation from raw lidar data: a labelling algorithm and its performance," *Photogramm. Eng. Remote Sens.* **71**(2), 217–226 (2005).
5. X. Liu, "Airborne LiDAR for DEM generation: some critical issues," *Prog. Phys. Geog.* **32**, 31–49 (2008).
6. M. Hollaus et al., "Airborne laser scanning and usefulness for hydrological models," *Adv. Geosci.* **5**, 57–63 (2005).
7. M. D. McCoy et al., "Airborne lidar survey of irrigated agricultural landscapes: an application of the slope contrast method," *J. Archaeol. Sci.* **38**(9), 2141–2154 (2011).
8. L. Jing et al., "Automated delineation of individual tree crowns from lidar data by multi-scale analysis and segmentation," *Photogramm. Eng. Remote Sens.* **78**(12), 1275–1284 (2012).
9. F. M. Southee et al., "Application of lidar terrain surfaces for soil moisture modeling," *Photogramm. Eng. Remote Sens.* **78**(12), 1241–1251.
10. K. D. Fieber et al., "Validation of canopy height profile methodology for small-footprint full-waveform airborne LiDAR data in a discontinuous canopy environment," *ISPRS J. Photogramm. Remote Sens.* **104**, 144–157 (2015).
11. A. Khosravipour et al., "Generating pit-free canopy height models from airborne lidar," *Photogramm. Eng. Remote Sens.* **80**(9), 863–872 (2014).
12. L. Cao et al., "Tree species classification in subtropical forests using small-footprint full-waveform LiDAR data," *Int. J. Appl. Earth Obs. Geoinf.* **49**, 39–51 (2016).
13. N. Csanyi and C. K. Toth, "Improvement of lidar data accuracy using lidar-specific ground targets," *Photogramm. Eng. Remote Sens.* **73**(4), 385–396 (2007).
14. S. Dahlqvist et al., "Evaluating the correctness of airborne laser scanning data heights using vehicle-based RTK and VRS GPS observations," *Remote Sens.* **3**(12), 1902–1913 (2011).
15. C. Hladik and M. Alber, "Accuracy assessment and correction of a LIDAR-derived salt marsh digital elevation model," *Remote Sens. Environ.* **121**, 224–235 (2012).
16. W. T. Tinkham et al., "A methodology to characterize vertical accuracies in Lidar-derived products at landscape scales," *Photogramm. Eng. Remote Sens.* **79**(8), 709–716 (2013).
17. R. Canavosio-Zuzelski et al., "Assessing Lidar accuracy with hexagonal retro-reflective targets," *Photogramm. Eng. Remote Sens.* **79**(8), 663–670 (2013).
18. S. Gould et al., "Influence of a dense, low-height shrub species on the accuracy of a LiDAR-derived DEM," *Photogramm. Eng. Remote Sens.* **79**(5), 421–431 (2013).
19. M. Isenburg, "LASzip," *Photogramm. Eng. Remote Sens.* **79**(2), 209–217 (2013).
20. A. Khosravipour et al., "Effect of slope on treetop detection using a LiDAR canopy height model," *ISPRS J. Photogramm. Remote Sens.* **104**, 44–52 (2015).
21. J. Rentsch and P. Krzystek, "Lidar strip adjustment with automatically reconstructed roof shapes," *Photogramm. Rec.* **27**(139), 272–292 (2013).
22. J. Höhle, "Assessing the positional accuracy of airborne laser scanning in urban areas," *Photogram. Rec.* **28**(142), 196–210 (2013).
23. Q. Lin et al., "Comparison of elevation derived from InSAR data with DEM over large relief terrain," *Int. J. Remote Sens.* **15**, 1775–1790 (1994).
24. A. P. Young et al., "Comparison of airborne and terrestrial lidar estimates of seacliff erosion in southern California," *Photogramm. Eng. Remote Sens.* **76**(4), 421–427 (2010).
25. J. Höhle and M. Höhle, "Accuracy assessment of digital elevation models by means of robust statistical methods," *ISPRS J. Photogramm. Remote Sens.* **64**, 398–406 (2009).

26. S. P. Wechsler and C. N. Kroll, "Quantifying DEM uncertainty and its effect on topographic parameters," *Photogramm. Eng. Remote Sens.* **72**(9), 1081–1090 (2006).
27. C. S. Yang et al., "Twelve different interpolation methods: a case study of surfer 8.0," in Proc. of the ISPRS XXth Congress, Istanbul, Turkey, pp. 778–783 (2004).
28. K. Jacobsen, "DEM generation from satellite data," in *EARSeL (Hrsg.)*, p. 4, Millpress, Ghent (2003).
29. ASPRS (American Society of Photogrammetry and Remote Sensing), ASPRS Guidelines Vertical Accuracy Reporting for Lidar Data, 2014, http://www.asprs.org/a/society/committees/lidar/Downloads/Vertical_Accuracy_Reporting_for_Lidar_Data.pdf (15 November 2014).
30. K. Jacobsen, "Characteristics of airborne and space-borne height models," in *Proc. of the EARSeL Symp.*, Matera, Italy (2013).
31. A. L. Montealegre et al., "Interpolation routines assessment in ALS-derived digital elevation models for forestry applications," *Remote Sens.* **7**, 8631–8654 (2015).

Umut Gunes Sefercik received his PhD from Bulent Ecevit University (BEU), Turkey, in 2010. He finished his postdoctoral at the National Center for Airborne Laser Mapping (NCALM), University of Houston, USA, in 2014. He is an associate professor at the Department of Geomatics Engineering, BEU. His research interests are processing, generation, and quality validation of airborne and spaceborne remote sensing data and products.

Gurcan Buyuksalih received his PhD from the Department of Geography and Topographic Science, University of Glasgow, UK. He is an associate professor in photogrammetry at Bimtas, Istanbul, Turkey. His research direction is the full range of photogrammetry, especially application of space imagery.

Karsten Jacobsen received his PhD in photogrammetry from Leibniz University Hannover, Germany. His main research area is numerical photogrammetry, especially the use of space imagery.

Mehmet Alkan received his PhD from Karadeniz Technical University (KTU), Turkey, in 2005. He is an associate professor at the Department of Geomatics Engineering, Yıldız Technical University. His research interests are database management, geographical information systems, remote sensing, object extraction, national spatial data infrastructure, e-municipality, and e-government.